Extreme Mechanics Letters 77 (2025) 102319

Contents lists available at ScienceDirect

Extreme Mechanics Letters

journal homepage: www.elsevier.com/locate/eml

Multi-axed phase-transforming cellular material: A data-driven design and validation using finite-element method and machine learning

Masayuki Okugawa [a,b,*], Sosuke Kanegae [a], Yuichiro Koizumi [a,b,*]

[a] Division of Materials and Manufacturing Science, Graduate School of Engineering, Osaka University, 2-1 Yamadaoka, Suita, Osaka 565-0871, Japan
[b] Anisotropic Design & Additive Manufacturing Research Center, Osaka University, 2-1 Yamadaoka, Suita, Osaka 565-0871, Japan

ARTICLE INFO

Keywords:
Mechanical metamaterial
Phase-transformation cellular material
3D printing
Bistability
Atom-mimetic

ABSTRACT

We developed the novel Atom-Mimetic Cube-Diagonally Multi-Axed Phase-Transforming Cellular Material (AMCDMA-PXCM), hereafter AM-PXCM for short, for a multi-axial bistable metamaterial designed with inspiration from a face-centered cubic (FCC) crystal structure: the designed AM-PXCM consists of spheres at atomic positions of structure and dogleg-shaped beams connecting nearest neighbor spheres. Stress-strain relationship of AM-PXCM was investigated by Finite Element Method (FEM) simulation. Analyzing the results by Logistic classification revealed that the mechanical properties significantly depend on the designing parameters and the distance between the beam and the tetrahedron (k) dominantly determines the bistability of the FCC-based AM-PXCM. In addition, combined with the machine learning method (i.e., inverse design), we succeeded to predict the designing parameters to have the desired mechanical properties for a bistable metamaterial. The designed AM-PXCMs were realized using a 3D printer and validified to show the predicted mechanical properties. This established method for developing AM-PXCM is suggested to be also applied to a development of an AM-PXCM with the symmetry of other crystal structures.

1. Introduction

Metamaterials are materials that create fine periodic structures on a directly controllable scale and develop properties that cannot be realized with existing materials [1,2]. For example, metamaterials exhibiting unique optical properties, such as negative index of refraction [3,4] and negative Poisson's ratio [5–7].

Phase-transforming cellular materials (PXCMs) [8], which are one kind of mechanical metamaterials, are attracting much attention because of their potential applications utilizing the bistability of their shape. PXCM has two stable configurations transformed from one phase to another phase by applying stress. This bistability enables us to use the PXCM as a repeatable shock absorber [9–11]. Many types of PXCMs have been suggested [12–16] based on the idea of mechanical behavior under one-directional load [17,18]. Recently, the PXCMs have been developed to exhibit bistability in several directions [19–23]. The multi-axed PXCMs are expected to be applied for curved shapes, such as human and car bodies, in which loads are not unidirectional. However, the application is a challenge because the conventional PXCMs show bistable only to the load axis within 5° from the ideal load axis [24]. Therefore, a novel strategy is required to design a multi-axed PXCM which is easy to apply to curved shapes.

In this study, we developed a novel design method for Atom-Mimetic Cube-Diagonally Multi-Axed Phase-Transforming Cellular Material (AMCDMA-PXCM), hereafter AM-PXCM for short, based on a face-centered cubic (FCC) structure. We designed a PXCM bistable in four directions by applying the knowledge of material science to design PXCMs with symmetry of atomic arrangements. We also aimed to clarify the relationship between the design parameters and mechanical properties and to achieve the desired mechanical properties.

2. Design of AM-PXCM

Fig. 1a shows the designed AM-PXCM structure based on the FCC structure (Fig. 1b). Spheres are placed at the corner of the tetrahedra which is corresponding to the position of atoms in the FCC structure and the edges of the tetrahedra structure as beams representing interatomic bonds by combining two sinusoidal beams (Fig. 1c–f). The FCC lattice is constructed using the two distinct tetrahedra as illustrated in Fig. 1g: the beams are bent toward the center of the tetrahedra colored by red. On

* Corresponding authors at: Division of Materials and Manufacturing Science, Graduate School of Engineering, Osaka University, 2-1 Yamadaoka, Suita, Osaka 565-0871, Japan.
E-mail addresses: okugawa@mat.eng.osaka-u.ac.jp (M. Okugawa), ykoizumi@mat.eng.osaka-u.ac.jp (Y. Koizumi).

https://doi.org/10.1016/j.eml.2025.102319
Received 7 May 2024; Received in revised form 22 December 2024; Accepted 15 March 2025
Available online 26 March 2025

the other hand, the beams are bent towards the opposite direction in the blue colored tetrahedra. The space group of this structure is $Fd\bar{3}m$ while that of atomic/ FCC structure is $Fm\bar{3}m$ because of the symmetry of the bended beams. The designed structure is expected to show multi-axial bistability to 4 three-fold rotation axes, i.e., $< 111 >$ directional axes, of FCC structure by deformation of tetrahedral structures shifts towards the bottom surface on the opposite side.

The designed structure can be defined by the five design parameters as shown in Fig. 1f: the radius of sphere R, the thickness of beam t, the distance between nearest neighboring spheres a, the angle between beam direction and sphere surface ϕ, and the distance between the center of the beam and the center of tetrahedron k. The shape of sinusoidal beams is defined by:

$$y = \frac{h}{2}\left\{1 - \cos\left(\frac{2\pi}{\lambda}(x - R\cos\phi\ \ )\right)\right\} + R\sin\phi \tag{1}$$

where h is the amplitude (peak to valley) of the sinusoidal beam and λ is the wavelength of sinusoidal beams. Two sinusoidal beams are connected at the dashed line which makes the whole curved beam mirror-symmetric at the dashed line. h and λ are expressed as follows:

$$h = \sqrt{\frac{2}{3}}k - R\sin\phi \tag{2}$$

$$\lambda = \frac{\sqrt{6}}{4}a - \frac{\sqrt{3}}{3}k - R\cos\phi. \tag{3}$$

The sinusoidal beam is a straight beam ($h = 0$) when

$$k = k_1 = \sqrt{\frac{3}{2}}R\sin\phi. \tag{4}$$

On the other hand, two joining points between the sphere and the sinusoidal beam and a joining point between two sinusoidal beams line up on a straight line when

$$k = k_2 = \frac{a}{2\sqrt{2}} - R\left(\sqrt{\frac{1}{3}}\cos\phi - \sqrt{\frac{2}{3}}\sin\phi\right). \tag{5}$$

We defined the geometry coefficient of the curved beam k_r using k_1 and k_2 as

$$k_r = \frac{k - k_1}{k_2 - k_1} \tag{6}$$

The curved beam is a more bent shape with smaller k_r and straighter with closing k_r to 1.

The most remarkable difference between this design and other multi-directional bistable structures is the number of directions that exhibit bistability: the AM-PXCM show bistability to the four directions, which is more than the three orthogonal directions of the previously suggested

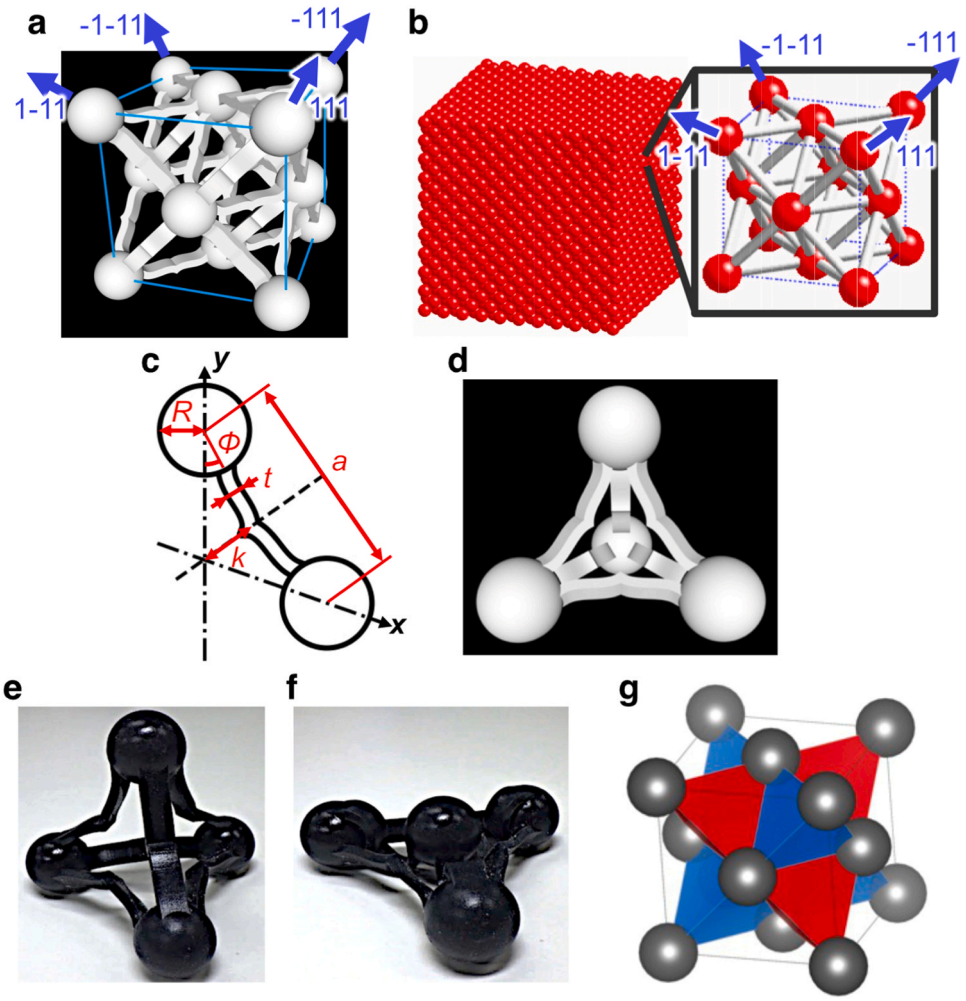

Fig. 1. (a) CAD model of the unit cell of AM-PXCM. Arrows indicate the direction of AM-PXCM exhibiting bistability, which is $< 111 >$ direction of FCC structure. (b) Schematic of FCC structure. (c) Drawing of a beam of AM-PXCM and (d) CAD model of a tetrahedral structure of AM-PXCM. (e, f) 3D printed tetrahedral structures of AM-PXCM before and after deformed by pressing one of the vertexes and stabilizes at a meta-stable phase. (g) FCC-lattice consisting of two distinct tetrahedra.

PCXM [12,20–22]. Moreover, the AM-PXCM can be transformed with the larger strain almost 100 %, as shown in Fig. 1b and c, compared to that up to 30 % of the conventional PXCMs, which are mostly composed of a cubic frame and curved bistable beams and can be transformed to a metastable state only by the amplitude of the curved beams [12,20–22].

3. Method

3.1. Finite element method simulations

Finite-element method (FEM) analysis has been performed using COMSOL software to investigate the mechanical response and deformation of AM-PXCM. The FEM model was simplified consisting of a beam and two spheres on both ends of the beam, as schematically illustrated in Fig. 1f. The model was compressed in $< 111 >$ direction by moving the sphere along the vertical dashed-dotted lines. Generally, a force-displacement relation is obtained by applying a load to a model in FEM simulations. On the other hand, a force-displacement relation of the structure with a snap buckling behavior cannot be obtained by the same way because of the decrease in force after a snap buckling. Therefore, a load-displacement curve was obtained using the displacement control method in this study: The displacement was gradually increased and the required load at each displacement was calculated. The sphere on the bottom end was fixed, and displacement was applied to the sphere on the top end downward by 0.01 mm per step until the apparent strain reached 1.5. The displacement d of the sphere and the applied force f are measured to evaluate the load-displacement relationship of the simplified model. The apparent stress ε and strain σ of AM-PXCM can be obtained by

$$\varepsilon[-] = \frac{d[\mathrm{m}]}{\sqrt{\frac{2}{3}}a[\mathrm{m}]} \tag{7}$$

$$\sigma[\mathrm{Nm}^{-2}] = \frac{3f[\mathrm{N}]}{\frac{\sqrt{3}}{4}\pi R[\mathrm{m}]^2 \times 2}. \tag{8}$$

Apparent Young's modulus E was calculated from the gradient of the stress-strain curve at $\varepsilon = 0$. In addition, the minimum and the maximum local stresses ($\sigma_{\max}$ and $\sigma_{\min}$) and local strains ($\varepsilon_{\max}$ and $\varepsilon_{\min}$) were evaluated to consider the effect of the designing parameters on strength, yield point, and bistability. The linear elastic material model was used for the simulation. The FEM simulations were conducted with a total number of 1225 using the parameters shown in Table 1.

In this study, we used two machine models, logistic regression and inverse design models, to analyze the relationship between the mechanical properties of the AM-PXCM and the design parameters. We performed logistic regression to understand the tendency of bistability qualitatively. Conversely, an inverse model analysis was conducted to predict and control the mechanical properties of the AM-PXCM.

Logistic regression analysis is a linear classification method that classifies datasets that whose data is labelled as 0 or 1 using the logistic function (Eq. (9)).

$$f(x) = \frac{1}{1+e^{-x}} \tag{9}$$

In this case, design parameters that were monostable were labelled as 0, and design parameters that were bistable were labelled "1".

Table 1
List of values for each design parameter.

Design parameter	value
R/t	4, 5, 6, 7, 8
a/R	6, 7, 8, 9, 10, 11, 12
ϕ	15, 22.5, 30, 37.5, 45
k_r	1/8, 1/4, 3/8, 1/2, 5/8, 3/4, 7/8

Explanatory variable for logistic regression analysis is represented by Eq. (10):

$$\boldsymbol{X} = \begin{bmatrix} R \\ a \\ \phi \\ k \end{bmatrix} \tag{10}$$

$\boldsymbol{X}$ was standardized and substituted for perceptron represented by Eq. (11):

$$\boldsymbol{Y} = f(\boldsymbol{X}^T\boldsymbol{W} + b) \tag{11}$$

where $\boldsymbol{Y}$ is the objective variable and is defined as $\boldsymbol{Y} = 1$ for bistable and $\boldsymbol{Y} = 0$ for monostable, $\boldsymbol{W}$ refers to the weights, and b represents the bias. The logistic regression model was trained, achieving an impressive accuracy of 96 %. The resulting weights $\boldsymbol{W}$ and bias b are given in Eq. (12):

$$\boldsymbol{W} = \begin{bmatrix} -0.50 \\ -6.60 \\ -1.62 \\ 9.58 \end{bmatrix}, \quad b = -1.61 \tag{12}$$

The design parameters are predicted to exhibit bistability are determined by Eqs. (13) and (14):

$$f(\boldsymbol{X}^T\boldsymbol{W} + b) \geq 0.5 \tag{13}$$

$$\boldsymbol{X}^T\boldsymbol{W} + b \geq 0 \tag{14}$$

Eq. (14) expresses the boundary condition for the bistability of the AM-PXCM.

3.2. Machine learning assisted optimization

We performed machine learning for the inverse estimation the design parameters of AM-PXCM with desired properties based on the FEM deformation analysis. The bistability is caused by snap-through; the two displacements are relative to the one stress and the relationship between displacements and the stress is nonlinear. Therefore, it is difficult to solve the inverse problem by an analytical model. Recently, machine learning methods have been recognized as a powerful tool for optimizing design parameters and introduced to material design [25] and metamaterial design [7,26]. Among them, we introduced the robust machine learning technique based on neural networks (NNs) that provides predictions for the inverse problem, i.e., Inverse design [27–30]. Inverse design contains two neural networks: forward neural network (f-NN) and inverse neural network (i-NN). The f-NN can predict mechanical properties from design parameters. On the other hand, the i-NN can predict design parameters from mechanical properties. In addition, the f-NN is also used to check the accuracy of i-NN in the inverse design [27].

Fig. 2 shows the schematic illustration of the inverse design [27]. First, explanatory variables are predicted from objective variables by i-NN with random initial weights. The predicted explanatory variables are next substituted to f-NN to reconstruct objective variables. The reconstructed objective variables are compared with the true objective variables. The error between the reconstructed value and the true value is calculated with the loss function. The weights and biases of i-NN are updated by the sensitivity. The inverse design model was trained by repeating this process and updating the weights of i-NN.

In the present study, the ReLU and the linear functions were used as activation functions for hidden layers and the output layers, respectively. First, the f-NN model was trained, and then the i-NN was trained with the verification using the trained f-NN as follows [27]:

(1) Solving the inverse problem using i-NN.
(2) Inputting the predicted design parameters to a pre-trained f-NN, and the properties are reconstructed.

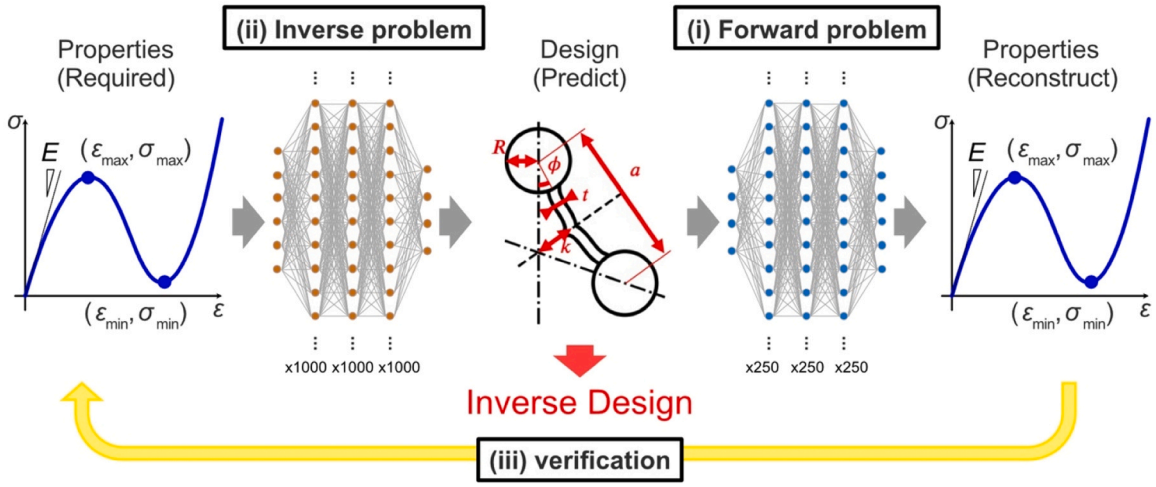

Fig. 2. Schematic of the inverse design process. The neural network for the inverse problems takes a queried mechanical property as input and output design parameters. The predicted design parameters are fed to the neural network for the forward problem to reconstruct mechanical properties and verify the predictions of the inverse problem. Both NN models consist of three hidden layers with the indicated number of nodes.

(3) Comparing the initially inputted and the reconstructed properties and coefficient of determination is evaluated.
(4) Updating the weights of i-NN using gradient descent based on the loss function.
(5) Repeating steps (1) to (4).

We trained the NNs using a data set of 1225 designs obtained by the FEM simulations with the parameters shown in Table 1. The NNs were optimized using the gradient descent method and validated by cross-validation method to achieve highly accurate learning with a small amount of data. In this study, we used the mean-squared error (MSE) as the loss function expressed as follows:

$$MSE = \frac{\sum_{i=1}^{n} (a_i - y_i)^2}{n} \# \tag{15}$$

where a_i and y_i are true and predicted values, respectively.

The hyperparameters of the number of hidden layers, the number of nodes per layer, the learning rate, and the number of cross-validation segments for f-NN and i-NN are optimized to have the maximized prediction accuracy and the minimized loss function. The 1050 combinations of the hyperparameters were tested, and Table 2 shows the optimized hyperparameters for f-NN and i-NN.

3.3. Experimental validation

The predicted AM-PXCMs were fabricated by the powder-bed fusion (PBF) type additive manufacturing, i.e., selective-laser sintering (SLS), using the polymer-PBF machine (Sinterit LISA) and thermoplastic polyurethane (TPU) powders (Sinterit FLEXA BRIGHT), which is a typical elastomer used in the PBF process. 2 AM-PXCMs were fabricated using the designing parameters shown in Table 3, which are expected to exhibit monostable and bistable mechanical properties. The compression tests of the fabricated AM-PXCM were performed using the universal testing machine (Shimadzu AG-IN 500 N) to investigate the deformation behavior and bistability. The built specimens were first compressed at a quasi-static compression rate of 0.5 mm/s up to a deformation of 15 mm. Then, the specimen was unloaded to the initial position with 0.5 mm/s. E, σ_{max}, σ_{min}, ε_{max}, and ε_{min} were evaluated.

Table 2
Hyperparameters for each neural network in the Inverse design process.

	Number of hidden layers	Number of nodes in hidden layer	Learning rate	Number of batches	Epochs
Forward problem	3	250	0.001	20	100
Inverse problem	3	1000	0.005	20	100

Table 3
Design parameter sets of atom-mimetic cube-diagonally multi-axed phase-transforming cellular material.

Design parameter	Parameter set A	Parameter set B
R/t	4	4
a/R	6	6
ϕ	45°	45°
k_r	7/8	1/2

4. Results and discussion

4.1. FEM analysis of deformation behavior of AM-PXCM

Fig. 3 shows the snapshots of the deformation behavior of a beam in a bistable AM-PXCM simulated by FEM for the cases of parameter set A (i.e., $t = 1$ mm, $R = 4$ mm, $a = 24$ mm, $\phi = 45°$, $k_r = 7/8$) (Fig. 3a1–a6) and parameter set B (i.e., $t = 1$ mm, $R = 4$ mm, $a = 24$ mm, $\phi = 45°$, $k_r = 1/2$) (Fig. 3b1–b6). Fig. 3a1–a5 show the shape of the model at the moments indicated by the points a1–a5 in the force-displacement curve Fig. 3a6, respectively. On the other hand, Fig. 3b1–b5 show the shapes of the model at the moments indicated by the points b1–b5 in the force-displacement curve (Fig. 3b1–b5), respectively. The colors of the images indicate the magnitude of von Mises stress. Fig. 3a1 and b1 show the original shape without any load. Fig. 3 a2 and b3 are for the moments where the load started to decrease after showing maximum. The elastic strain energy is maximum when the slope of the load-displacement curve is negative, and the load is zero. Then, the von Mises stress at this point is the maximum value. It is noted that the beam is bent so that the center point of the beam goes up in the case of parameter set A (Fig. 3a2), while the beam is bent so that the center point of the beam goes down in the case of parameter set B (Fig. 3b2) at the beginning of the deformation. However, the center points go down finally in both cases of parameter sets A and B. The difference in the stability of the deformed shape seems to be related to the change in the direction of movement of the midpoint of the beam. In the case where

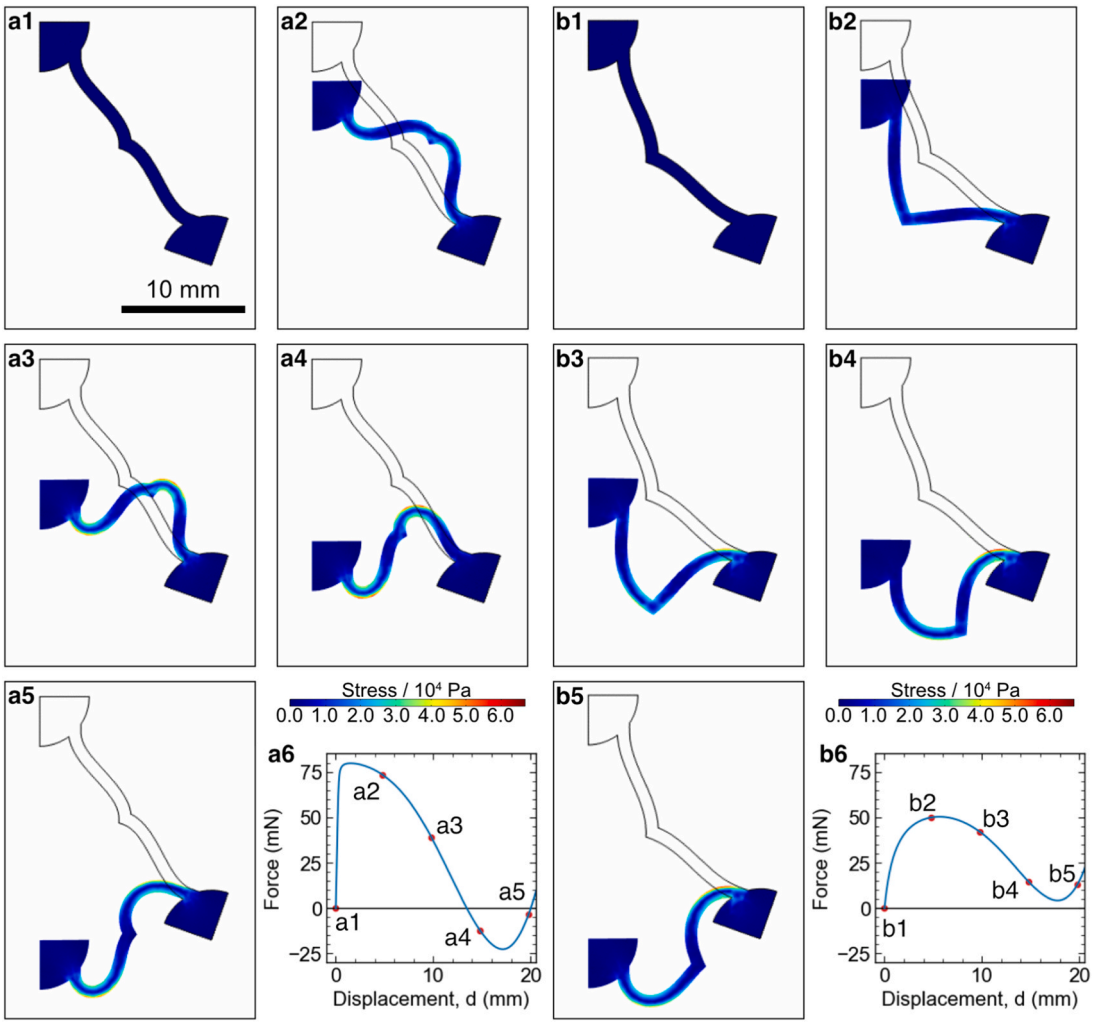

Fig. 3. (a1–5) Deformation behavior of a beam in a bistable AM-PXCM. (a6) Force-displacement relationship of a beam in a bistable AM-PXCM. (b1–5) Deformation behavior of a beam in a monostable AM-PXCM. (b6) Force-displacement relationship of a beam in a monostable AM-PXCM.

the beam bends to move over the center of the beam during the deformation process (parameter set A, Fig. 3a2), the beam bends in such a way that it buckles. In the initial stage of deformation, axial compressive deformation of the beam is considered to be the dominant deformation mode. On the other hand, in the case where the beam bends down the center of the beam (parameter set B, Fig. 3b2), the dominant deformation mode is the bending deformation of the beam. This difference in deformation mode is considered to cause a large difference in apparent Young's modulus (Fig. 3a6 and b6).

Fig. 4 shows E, ε_{max}, σ_{max}, ε_{min}, σ_{min}, and ρ plotted as a function of the design parameters of R/t (the radius of spheres with respect to the thickness of the beam), a/R (the distance between adjacent spheres with respect to the radius of spheres), ϕ and k_r (the degree of straightness of the beam). These design parameters influence the mechanical properties and density of the AM-PXCM. However, the multiple parameters are mutually influencing each other, making it difficult to express the characteristics as functions of each parameter.

The bistability of PXCM is determined by the sign (i.e., positive, or negative) of the stress of the minima. When the stress of the minima is positive, no metastable state exists, and therefore, PXCM is monostable. On the other hand, when the stress of minima is negative, a metastable state appears, therefore, PXCM becomes bistable. Fig. 5 shows $\sigma_{min}/\sigma_{max}$ plotted as a function of the design parameters of R/t, a/R, ϕ, and k_r. The stress of maxima σ_{max} represents the strength, and $\sigma_{min}/\sigma_{max}$ is considered to ignore the strength and represent the bistability. According to the graph bistability barely depends on design parameters R/t, a/R, and ϕ, but strongly depends on k_r (the degree of straightness of the beam). The threshold of bistability was $k_r \sim 0.52$. When $\sigma_{min} / \sigma_{max}$ has a negative value with a large absolute value, the energy barrier between the stable state and metastable state becomes larger. Therefore, the metastable state is most stable at $k_r = 3/4$.

Fig. 6 shows three-dimensional plots of the design parameter sets colored by the bistability result of the parameter set. The design parameter sets that were monostable are plotted in blue, and the design parameter sets that were bistable are plotted in red. The planar boundary between monostable and bistable was determined by logistic regression and plotted as a blue surface. Substituting the trained weights and bias, the boundary condition resulted in Eq. (15):

$$-0.50\,R^* - 6.60\,a^* - 1.62\,\phi^* + 9.58\,k^* \geq 1.61 \tag{16}$$

where R^*, a^*, ϕ^*, and k^* are normalized R, a, ϕ, and k, respectively, and those values were scaled in the ranged from 0 to 1. The coefficients can be interpreted as the magnitude of the contributions to the bistability. The analysis revealed that k and a have large contributions. Therefore, AM-PXCM tends to be bistable with larger k which has a positive coefficient, and smaller a which has a negative coefficient.

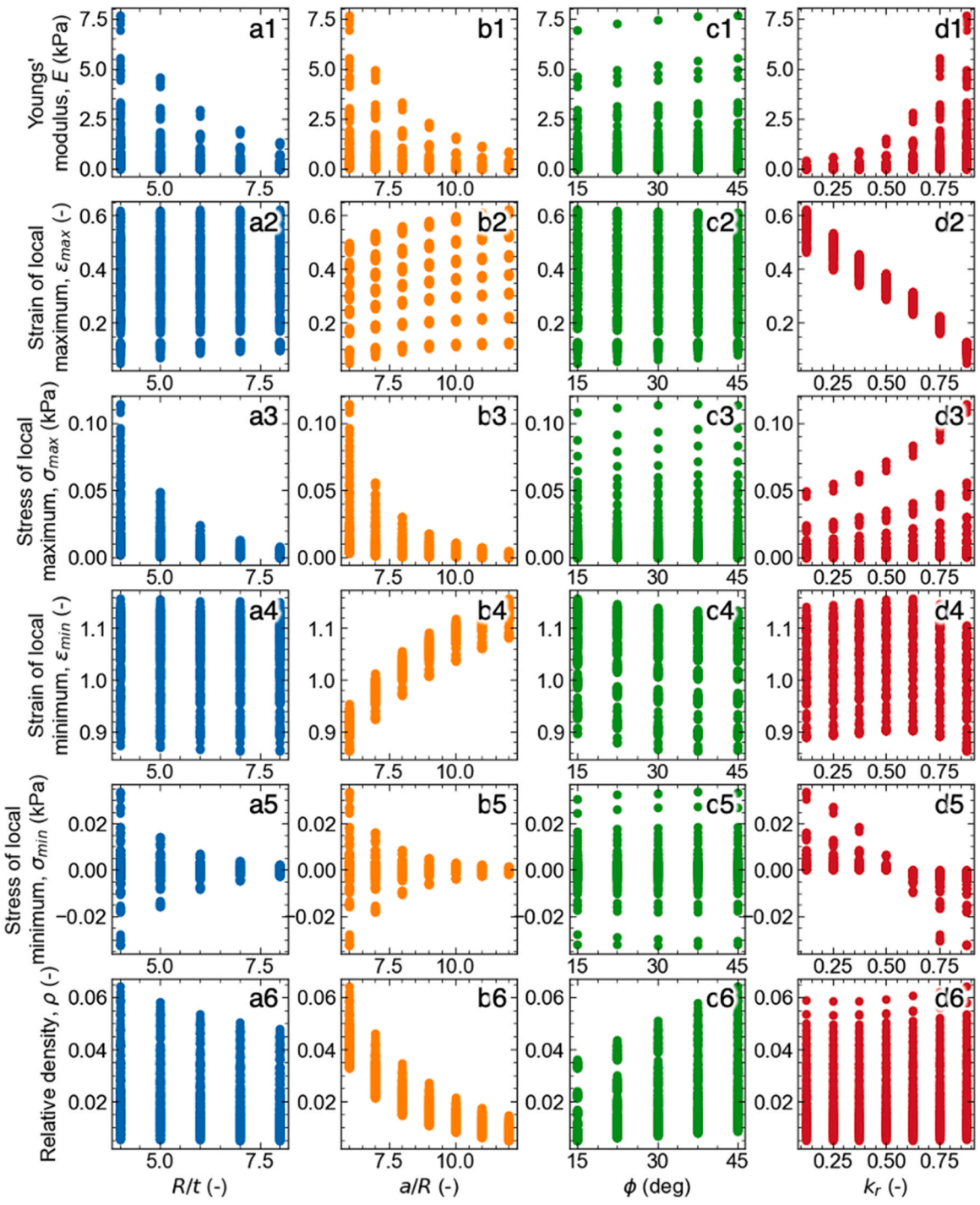

Fig. 4. Relation between mechanical properties of AM-PXCM and design parameters evaluated by FEM simulation: (a) effect of R/t, (b) a/R, (c) ϕ, and (d) k_r.

4.2. Prediction design parameters to have desired mechanical properties and experimental verification

To control the mechanical properties of the AM-PXCM to the desired ones by properly selecting parameters in the large design parameter space, the results are analyzed by the Inverse design method [27]. Fig. 7 shows the correlations between the true values and the predicted values obtained using the trained f-NN (Fig. 7a-f) and i-NN (Fig. 7g–j). The coefficients of determination (CoD, R^2) for f-NN are all high enough to conclude that the mechanical properties of the AM-PXCM can be predicted with sufficient accuracy with an error range of smaller than 0.1 %. On the other hand, the CoD for i-NN were all lower than those for the f-NN, but the prediction accuracy of the i-NN is still high, with an error range of less than 0.1 %. This suggests that the i-NN able to predict the optimal design parameters to achieve the desired mechanical properties accurately. The i-NN provides a more comprehensive understanding of the design space and the trade-offs between different design parameters, allowing for the identification of designs that balance performance and manufacturability.

The AM-PXCMs with monostable and bistable properties were fabricated using the SLS-type 3D printer for verification using the design parameters shown in Table 3. The lattice of Sample A created with Parameter set A has a relatively small bending of the beam. On the other hand, the lattice of Sample B made with Parameter set B has a large

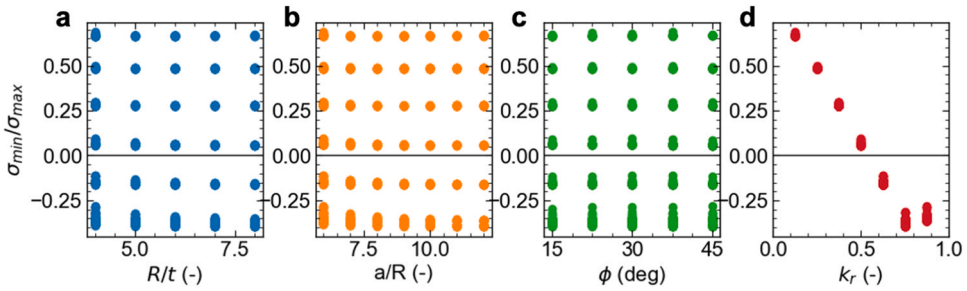

Fig. 5. Dependence of the ratio of minima stress to maxima stress on the design parameters on (a) R/t, (b) a/R, (c) ϕ, and (d) k_r.

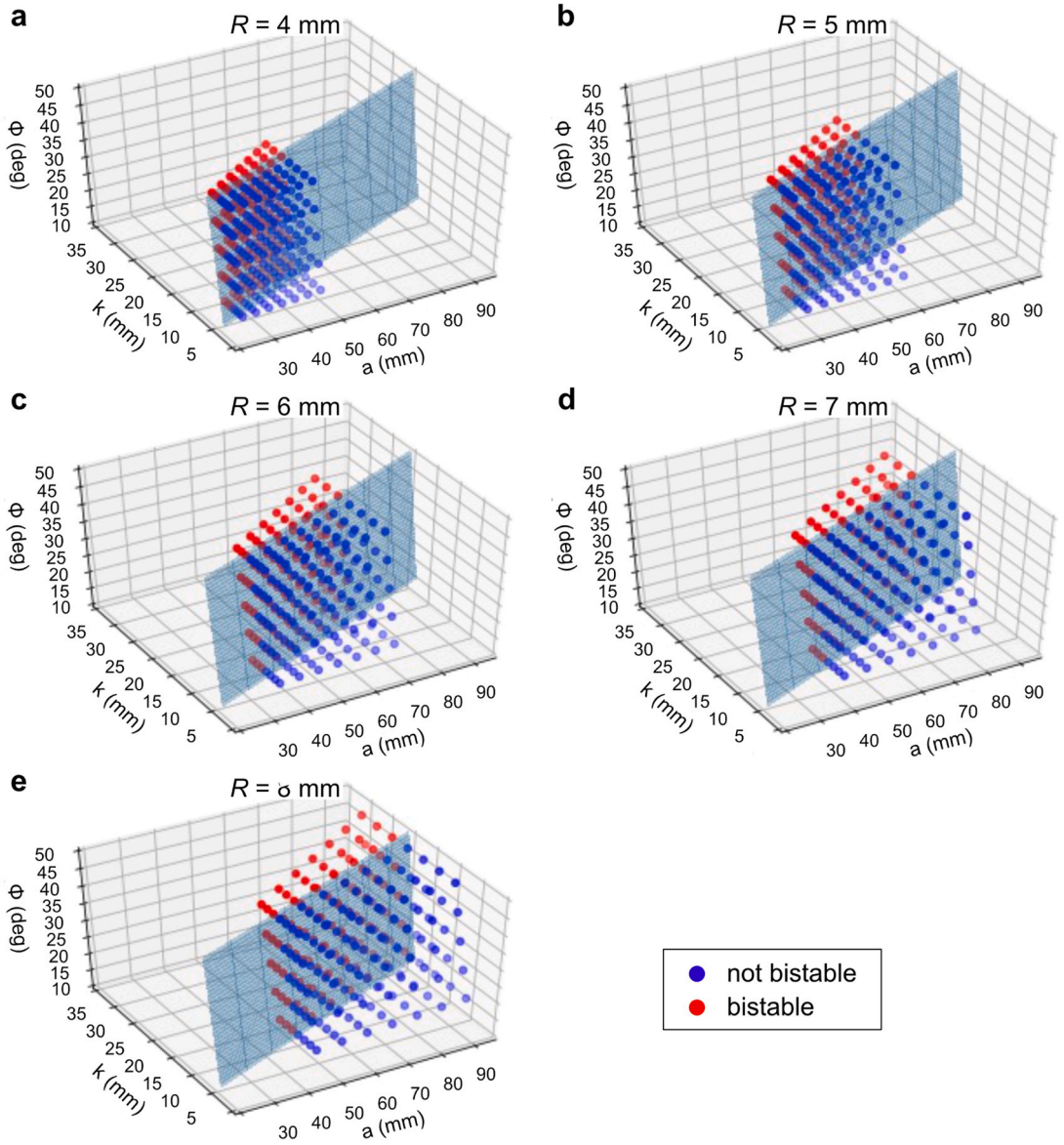

Fig. 6. 3D plots of bistability and boundary plane determined by logistic regression. (a) R = 4 mm, (b) 5 mm, (c) 6 mm, (d) 7 mm, and (e) 8 mm.

bending of the beam. Fig. 8 shows the load-displacement curves of the AM-PXCMs under compression and unloading tests and the corresponding snapshots. In the deformation of the sample A (Fig. 8a1–a12), the load increased greatly at the initial stage of deformation and then deformed with buckling as seen in Fig. 8a5 (corresponding to the point a5 in Fig. 8a3). This lattice exhibited bistability as expected in the simulation. Correspondingly, the stress became negative at the point of e where the lattice became compacted and horizontally flat as seen in Fig. 8a8 in the experiment after the buckling, indicating a metastable state in compression. In Sample B (Fig. 8b1–b12), the beam, which originally had a large bending, increased the bending angle from the initial stage of deformation. This deformation is easy, and the load is relatively small. As expected by the simulation, the lattice of sample B exhibited no bistability, and the load never went to zero. Thus, the

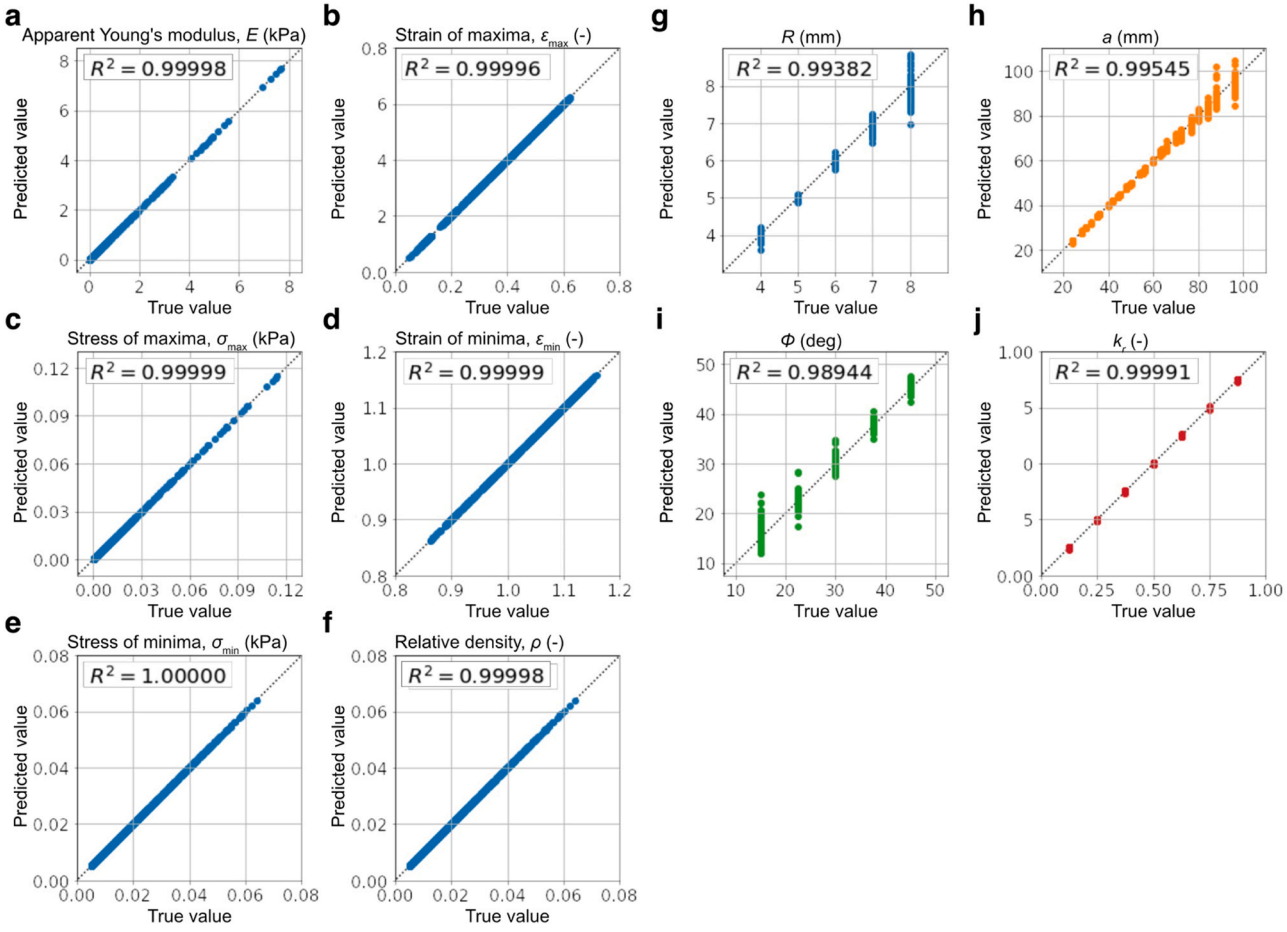

Fig. 7. (a)-(f) True vs. f-NN reconstructed mechanical properties. (g)-(j) true vs. i-NN predicted design parameters.

deformation behavior greatly differs depending on the difference in the bending of the beam. A clear difference, i.e., the presence or absence of bistability, arose as the result of the difference in the bending of the beams.

Overall, the results of our inverse design model demonstrate the potential of machine learning techniques to accelerate the development of new mechanical metamaterials with tailored properties. The accuracy of our model suggests that it can be applied to the design of a wide range of metamaterials with different geometries and mechanical properties. The investigation of the deformation behavior of larger AM-PXCM fabrications and its FEM simulation using a representative volume element model for more accurate prediction of the large deformation behavior are currently underway.

5. Conclusion

In this study, we developed the novel Atom-Mimetic Phase-Transforming Cellular Material (AM-PXCM) with a cube-diagonally multi-axed structure based on the face-centered cubic (FCC) crystal structure. The mechanical properties of the AM-PXCM were investigated by the Finite Element Method (FEM) simulations, and it has been found that the designing parameters, especially the bending of the beams, played a dominant role in determining the bistability of the material. By applying machine learning techniques, specifically the inverse design method, we were able to predict the designing parameters that would yield the desired mechanical properties for a bistable metamaterial. The accuracy of the predictions was verified through the actual fabrication and testing of AM-PXCM samples fabricated with a thermo-plastic polyurethane by a 3D printer. The experimental results matched reasonably with the predicted mechanical properties, confirming the effectiveness of our approach.

This study demonstrated the potential of AM-PXCM as a multi-axial bistable metamaterial with controllable mechanical properties. It has been demonstrated that it is possible to tailor apparent Young's modulus, stress-strain relationship, and bistability of the material by manipulating the design parameters, such as the radius of spheres, the thickness of beams, the distance between neighboring spheres, the angle between beam direction and sphere surface, and the distance between the center of the beam and the center of the tetrahedron, (i.e., the straightness of the beam). The inverse design method proved to be a powerful tool for predicting the optimal design parameters, enabling the efficient development of AM-PXCMs with desired mechanical properties.

Our research contributes to the advancement of mechanical metamaterials and expands their potential applications. The ability to design and fabricate multi-axial bistable metamaterials opens up new possibilities in areas such as shock absorbers, energy absorption, and flexible structures. Furthermore, the insights gained from this study can be applied to the development of AM-PXCMs based on other crystal structures, providing a framework for the design of metamaterials with a wide range of properties.

This study provides a comprehensive understanding of the relationship between the design parameters and mechanical properties of AM-PXCMs. The combination of FEM simulations and machine learning techniques offers a powerful approach to the efficient design and development of metamaterials with tailored properties. We believe that our findings will contribute to the advancement of materials science and engineering and inspire further research in the field of multi-axial

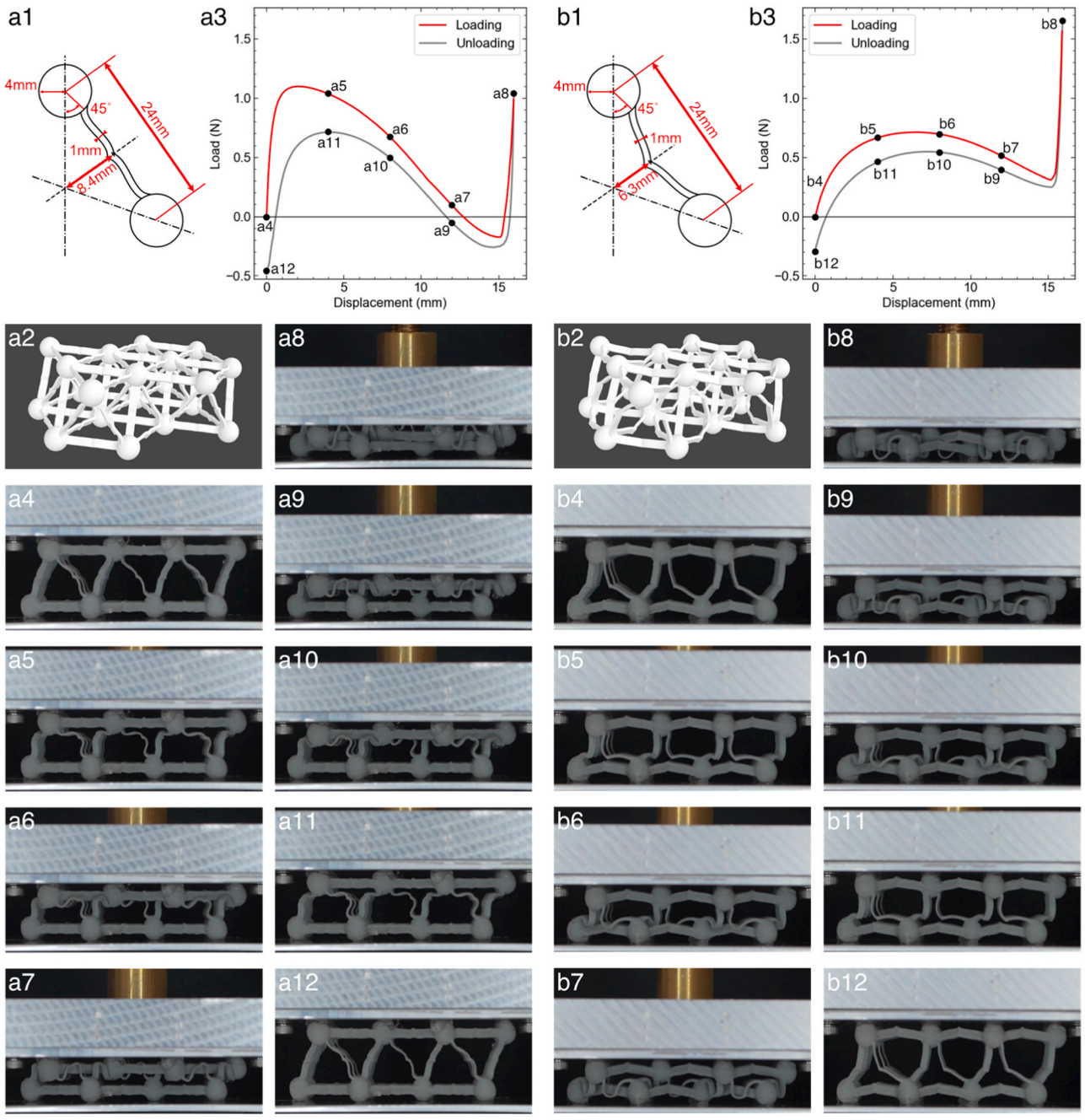

Fig. 8. (a1–a2, b1–b2) Schematic illustrations of beams and 3D-CAD model of AM-PXCMs. (a3, b3) Force-displacement relationships of the 3D printed AM-PXCMs and (a4–a12, b4–b12) snapshots at the strains indicated in a3 and b3. The design parameters were (a1–a12) the set A: $t = 1$ mm, $R = 4$ mm, $a = 24$ mm, $\phi = 45^{\circ}$, $k_r = 7/8$) and (b1–b12) the set B: $t = 1$ mm, $R = 4$ mm, $a = 24$ mm, $\phi = 45^{\circ}$, $k_r = 1/2$.

bistable metamaterials.

CRediT authorship contribution statement

Masayuki Okugawa: Writing – original draft, Writing – review & editing, Methodology, Visualization, Conceptualization. **Sosuke Kanegae:** Writing – original draft, Writing – review & editing, Software, Methodology, Investigation, Visualization, Funding acquisition, Conceptualization. **Yuichiro Koizumi:** Writing – original draft, Writing – review & editing, Methodology, Supervision, Funding acquisition, Project administration, Conceptualization.

Declaration of Competing Interest

The authors declare that they have no known competing financial interests or personal relationships that could have appeared to influence the work reported in this paper.

Acknowledgment

This work was partly supported by JSPS KAKENHI Grant Nos. 19K22063, 21J20611, 21H05018, 21H05193, and 22K18889.

Data availability

Data will be made available on request.

References

[1] J.U. Surjadi, L. Gao, H. Du, X. Li, X. Xiong, N.X. Fang, Y. Lu, Mechanical metamaterials and their engineering applications, Adv. Eng. Mater. 21 (2019) 1800864, https://doi.org/10.1002/adem.201800864.

[2] M. Askari, D.A. Hutchins, P.J. Thomas, L. Astolfi, R.L. Watson, M. Abdi, M. Ricci, S. Laureti, L. Nie, S. Freear, R. Wildman, C. Tuck, M. Clarke, E. Woods, A.T. Clare, Additive manufacturing of metamaterials: a review, Addit. Manuf. 36 (2020) 101562, https://doi.org/10.1016/j.addma.2020.101562.

[3] R.A. Shelby, D.R. Smith, S. Schultz, Experimental verification of a negative index of refraction, Science 292 (2001) 77–79, https://doi.org/10.1126/science.1058847.

[4] G. Zhao, S. Bi, Design and verification of double band negative refraction metamaterial, Chem. Phys. Lett. 725 (2019) 92–96, https://doi.org/10.1016/j.cplett.2019.04.020.

[5] X. Ren, R. Das, P. Tran, T.D. Ngo, Y.M. Xie, Auxetic metamaterials and structures: a review, Smart Mater. Struct. 27 (2018) 023001, https://doi.org/10.1088/1361-665X/aaa61c.

[6] H. Yang, L. Ma, Design and characterization of axisymmetric auxetic metamaterials, Compos. Struct. 249 (2020) 112560, https://doi.org/10.1016/j.compstruct.2020.112560.

[7] J.K. Wilt, C. Yang, G.X. Gu, Accelerating auxetic metamaterial design with deep learning, Adv. Eng. Mater. 22 (2020) 1901266, https://doi.org/10.1002/adem.201901266.

[8] D. Restrepo, N.D. Mankame, P.D. Zavattieri, Phase transforming cellular materials, Extrem. Mech. Lett. 4 (2015) 52–60, https://doi.org/10.1016/j.eml.2015.08.001.

[9] C.S. Ha, R.S. Lakes, M.E. Plesha, Design, fabrication, and analysis of lattice exhibiting energy absorption via snap-through behavior, Mater. Des. 141 (2018) 426–437, https://doi.org/10.1016/j.matdes.2017.12.050.

[10] D.M. Correa, T. Klatt, S. Cortes, M. Haberman, D. Kovar, C. Seepersad, Negative stiffness honeycombs for recoverable shock isolation, Rapid Prototyp. J. 21 (2015) 193–200, https://doi.org/10.1108/RPJ-12-2014-0182.

[11] T. Frenzel, C. Findeisen, M. Kadic, P. Gumbsch, M. Wegener, Tailored Buckling Microlattices as Reusable Light-Weight Shock Absorbers, Adv. Mater. 28 (2016) 5865–5870, https://doi.org/10.1002/adma.201600610.

[12] F. Pan, Y. Li, Z. Li, J. Yang, B. Liu, Y. Chen, 3D pixel mechanical metamaterials, Adv. Mater. 31 (2019) 1900548, https://doi.org/10.1002/adma.201900548.

[13] D.M. Correa, C.C. Seepersad, M.R. Haberman, Mechanical design of negative stiffness honeycomb materials, Integr. Mater. Manuf. Innov. 4 (2015) 165–175, https://doi.org/10.1186/s40192-015-0038-8.

[14] D.A. Debeau, C.C. Seepersad, M.R. Haberman, Impact behavior of negative stiffness honeycomb materials, J. Mater. Res. 33 (2018) 290–299, https://doi.org/10.1557/jmr.2018.7.

[15] S. Kanegae, M. Okugawa, Y. Koizumi, Martensitic phase-transforming metamaterial: concept and model, Materials 16 (2023) 6854, https://doi.org/10.3390/ma16216854.

[16] H. Nagayama, S. Kanegae, M. Hosoda, M. Okugawa, Y. Koizumi, Thermally induced phase transforming cellular lattice driven by bimetal beams, MRS Adv. 7 (2022) 701–705, https://doi.org/10.1557/s43580-022-00334-y.

[17] J. Qiu, J.H. Lang, A.H. Slocum, A Curved-Beam Bistable Mechanism, J. Micro Syst. 13 (2004) 137–146, https://doi.org/10.1109/JMEMS.2004.825308.

[18] B. Camescasse, A. Fernandes, J. Pouget, Bistable buckled beam: Elastica modeling and analysis of static actuation, Int. J. Solids Struct. 50 (2013) 2881–2893, https://doi.org/10.1016/j.ijsolstr.2013.05.005.

[19] H. Yang, L. Ma, Angle-dependent transitions between structural bistability and multistability, Adv. Eng. Mater. 22 (2020) 1900871, https://doi.org/10.1002/adem.201900871.

[20] X. Tan, B. Wang, S. Zhu, S. Chen, K. Yao, P. Xu, L. Wu, Y. Sun, Novel multidirectional negative stiffness mechanical metamaterials, Smart Mater. Struct. 29 (2020) 015037, https://doi.org/10.1088/1361-665X/ab47d9.

[21] H. Yang, L. Ma, 1D to 3D multi-stable architected materials with zero Poisson's ratio and controllable thermal expansion, Mater. Des. 188 (2020) 108430, https://doi.org/10.1016/j.matdes.2019.108430.

[22] C.S. Ha, R.S. Lakes, M.E. Plesha, Cubic negative stiffness lattice structure for energy absorption: Numerical and experimental studies International Journal of Solids and Structures Cubic negative stiffness lattice structure for energy absorption: Numerical and experimental studies, Int. J. Solids Struct. 178–179 (2019) 127–135, https://doi.org/10.1016/j.ijsolstr.2019.06.024.

[23] C. Ren, D. Yang, H. Qin, Mechanical performance of multidirectional buckling-based negative stiffness metamaterials: an analytical and numerical study, Materials 11 (2018) 1078, https://doi.org/10.3390/ma11071078.

[24] Y. Zhang, D. Restrepo, M. Velay-Lizancos, N.D. Mankame, P.D. Zavattieri, Energy dissipation in functionally two-dimensional phase transforming cellular materials, Sci. Rep. 9 (2019) 12581, https://doi.org/10.1038/s41598-019-48581-8.

[25] H. Fujii, D.J.C. Mackay, H.K.D.H. Bhadeshia, Bayesian neural network analysis of fatigue crack growth rate in nickel base superalloys, ISIJ Int 36 (1996) 1373–1382, https://doi.org/10.2355/isijinternational.36.1373.

[26] A. Bacigalupo, G. Gnecco, M. Lepidi, L. Gambarotta, Machine-learning techniques for the optimal design of acoustic metamaterials, J. Optim. Theory Appl. 187 (2020) 630–653, https://doi.org/10.1007/s10957-019-01614-8.

[27] S. Kumar, S. Tan, L. Zheng, D.M. Kochmann, Inverse-designed spinodoid metamaterials, Npj Comput. Mater. 6 (2020) 1–10, https://doi.org/10.1038/s41524-020-0341-6.

[28] B. Kim, S. Lee, J. Kim, Inverse design of porous materials using artificial neural networks, Sci. Adv. 6 (2020) 1–8, https://doi.org/10.1126/sciadv.aax9324.

[29] X. Zheng, X. Zhang, T.Te Chen, I. Watanabe, Deep learning in mechanical metamaterials: from prediction and generation to inverse design, Adv. Mater. 35 (2023), https://doi.org/10.1002/adma.202302530.

[30] K. Zhang, Y. Guo, X. Liu, F. Hong, X. Hou, Z. Deng, Deep learning-based inverse design of lattice metamaterials for tuning bandgap, Extrem. Mech. Lett. 69 (2024) 102165, https://doi.org/10.1016/j.eml.2024.102165.